Methods

1. Sampling

Paleomagnetic cores were drilled in the field with a water-cooled portable petrol-powered drill, and oriented in situ with both magnetic and sun compasses. Cores were subsequently cut in the lab into standard paleomagnetic specimens (25 x 22 mm). At the Sangsang ophiolite, we sampled seven sites from mantle hosted doleritic dykes distributed along a 300 m long section (see Table DR1). At each site, a variable number of cores (5 to 26) were collected within contiguous, discrete dykes.

At the Qunrang ophiolite, both the mantle and the crustal sections were sampled. Samples from the mantle section were collected from gabbro pods intruding the serpentinites. Four sites within discrete gabbro intrusions exposed over a ~200 m^2 area were sampled (see Table DR1). At each site, 11 to 24 cores were drilled homogeneously distributed within the intrusion. One single site within the crustal section, represented by sheeted sills, was drilled over a ~100 m long section. One core per sill was drilled at this doleritic sequence, consisting of multiple intrusions of sills with well-developed chilled margins.

2. Analysis of the natural remanent magnetization (NRM)

Natural remanent magnetization (NRM) of samples was investigated through thermal or alternating field (AF) demagnetization technique. AF demagnetization was carried out with an in-house developed robotized sample handler (Mullender et al., 2005) attached to a horizontal pass-through 2G Enterprises DC SQUID magnetometer (noise level 1-2 × 10^{-12} Am^2) hosted in a magnetically shielded room (residual field < 200 nT) at the Fort Hoofddijk Paleomagnetic Laboratory, Utrecht University (The Netherlands). Specimens were progressively demagnetized by 15 successive AF steps from 5 to 100 mT. About 10% of the samples was demagnetized with thermal treatment in a magnetically shielded oven (ASC, model TD48-SC) that has a < 10 nT residual field. NRM was measured after each demagnetization step with a horizontal 2G Enterprises DC SQUID magnetometer (noise level 3 × 10^{-12} Am^2). Specimens were progressively demagnetized by 12-13 successive temperature steps from 100 to 600°C, until complete demagnetization of the NRM.

Demagnetization data were plotted on orthogonal diagrams (Zijderveld, 1967), and the magnetization components isolated via principal component analysis (Kirschvink, 1980) using Remasoft 3.0 software (Chadima and Hrouda, 2006). Only computed directions showing maximum angle of deviation (MAD, Kirschvink (1980)) smaller than 15° were considered for this study. Site-mean directions were evaluated using a Fisherian statistics (Fisher, 1953) of virtual geomagnetic poles (VGPs) corresponding to the characteristic remanent magnetizations (ChRMs), adopting a fixed 45° cut-off (Johnson et al., 2008). The use of VGPs rather than paleomagnetic directions for the computation of the site mean values was preferred as it allows a more realistic error estimate on the declination and inclination values (Deenen et al., 2011). The VGP scatter (i.e., A_{95}) obtained at each site was compared to the expected scatter induced by paleosecular variation (PSV) of the geomagnetic field (constrained by a minimum - A_{95min} - and a maximum - A_{95max} - value) to assess whether PSV is

represented (Deenen et al., 2011). $A_{95} < A_{95min}$ indicates that PSV is not adequately represented, likely due to a not sufficient time averaging or remagnetization. Conversely, $A_{95} > A_{95max}$ may point out to additional processes (i.e., tectonics) responsible for the enhanced scatter.

3. Curie balance experiments

Thermomagnetic experiments consisted in measuring the variation of the remanence during stepwise heating-cooling cycles with an in-house developed Curie balance with instrumental sensitivity of $2 \cdot 10^{-9}$ Am^2. The interpretation of the curves allows identification of the blocking temperature(s) and main mineralogical changes upon heating.

4. Microscopy

Microstructures were examined in polished thin section using a classic polarized light microscopy. Back-scattered electron (BSE) images were acquired using a JEOL JCM-6000 (Utrecht University, The Netherlands) scanning electron microscope (SEM). Qualitative elemental analyses were performed using an energy dispersive X-ray spectrometer (EDS) coupled with the SEM. Elemental analyses were performed both on spots and whole images allowing the definition of compositional maps.

5. Monte Carlo modeling

Computation of the rotation axis using the intersection between the fault plane and the bisectrix plane of the paleomagnetic vectors was iterated 500 times using a Monte Carlo approach. First, 500 pairs of points randomly distributed within the α_{95} cones of confidence of the rotated block (RB) and fixed block (FB) vectors at each locality were selected to generate 500 permissible great circle bisectrices (Fig. S7a, f). Then, 500 permissible fault planes were randomly generated using an arbitrary $\alpha_{95} = 5.0°$ error centered on the measured fault plane pole. The intersection between the 500 randomly generated bisectrices and fault planes yielded 500 statistically acceptable estimates of the rotation axis orientation and magnitude of rotation, displayed as contour diagrams (Fig. S7b, g), and frequency distribution histograms (Fig. S7e, l), respectively.

6. Calculation of the original rotation axis direction

The original direction of the rotation axes before the Cenozoic deformation associated to the India-Asia collision was inferred by correcting the calculated (in situ) rotation axes for the local deformation (both tilt and rotation).

At the Sangsang area, the obtained rotation axes were (step 1) first corrected for the local tilt inferred from the bedding of the Xigaze Group (265°/76° N) unconformably covering the ophiolite, by restoring this unit to horizontal. Then (step 2), we rotated along a vertical axis the obtained axes by 9° clockwise (CW) to remove an equal amount of counterclockwise (CCW) vertical-axis rotation documented by Huang et al., (2015) from the Xigaze Group sediments.

At the Qunrang area, we adopted a similar strategy removing the local tilt of the Xigaze Group (265°/100° N) by restoring it to the horizontal, and the regional 85° of CCW vertical-axis rotation documented by Pozzi et al. (1984) and Abrajevitch et al. (2005), and Huang et al. (2015).

References Cited

Abrajevitch, A., Ali, J., Aitchison, J., Badengzhu, Davis, A., Liu, J., and Ziabrev, S., 2005, Neotethys and the India–Asia collision: Insights from a palaeomagnetic study of the Dazhuqu ophiolite, southern Tibet: Earth and Planetary Science Letters, v. 233, no. 1-2, p. 87-102.

Chadima, M., Hrouda, F. 2006. Remasoft 3.0 a user-friendly paleomagnetic data browser and analyzer. Travaux Géophysiques, XXVII, 20-21.

Deenen, M. H. L., Langereis, C. G., van Hinsbergen, D. J. J., and Biggin, A. J., 2011, Geomagnetic secular variation and the statistics of palaeomagnetic directions: Geophysical Journal International, v. 186, no. 2, p. 509-520.

Fisher, R. A., 1953, Dispersion on a sphere: Proc. R. Soc. London, v. 217, p. 295-305.

Johnson, C. L., Constable, C. G., Tauxe, L., Barendregt, R., Brown, L. L., Coe, R. S., Layer, P., Mejia, V., Opdyke, N. D., Singer, B. S., Staudigel, H., and Stone, D. B., 2008, Recent investigations of the 0-5 Ma geomagnetic field recorded by lava flows: Geochemistry, Geophysics, Geosystems, v. 9, no. 4.

Kirschvink, J. L., 1980, The least-squares line and plane and the analysis of palaeomagnetic data: Geophysical Journal, Royal Astronomical Society, v. 62, no. 3, p. 699-718.

Mullender, T. A. T., T. Frederichs, C. Hilgenfeldt, K. Fabian, and M. J. Dekkers (2005), Fully automated demagnetization and measurement of NRM, ARM and IRM on a '2G' SQUID magnetometer, IAGA, abstract number: IAGA2005-A-00898.

Pozzi, J. P., Westphal, M., Girardeau, J., Besse, J., Yao Xiu, Z., Xian Yao, C., and Li Sheng, X., 1984, Paleomagnetism of the Xigaze ophiolite and flysch (Yarlung Zangbo suture zone, southern Tibet): latitude and direction of spreading: Earth and Planetary Science Letters, v. 70, no. 2, p. 383-394.

Zijderveld, J.D.A., 1967. A.C. demagnetization of rocks: Analysis of results. In: Collinson, D.W., Creer, K.M., Runcorn, S.K., (eds). Methods in Palaeomagnetism. Elsevier, New York, pp 254-286.

Figure DR1

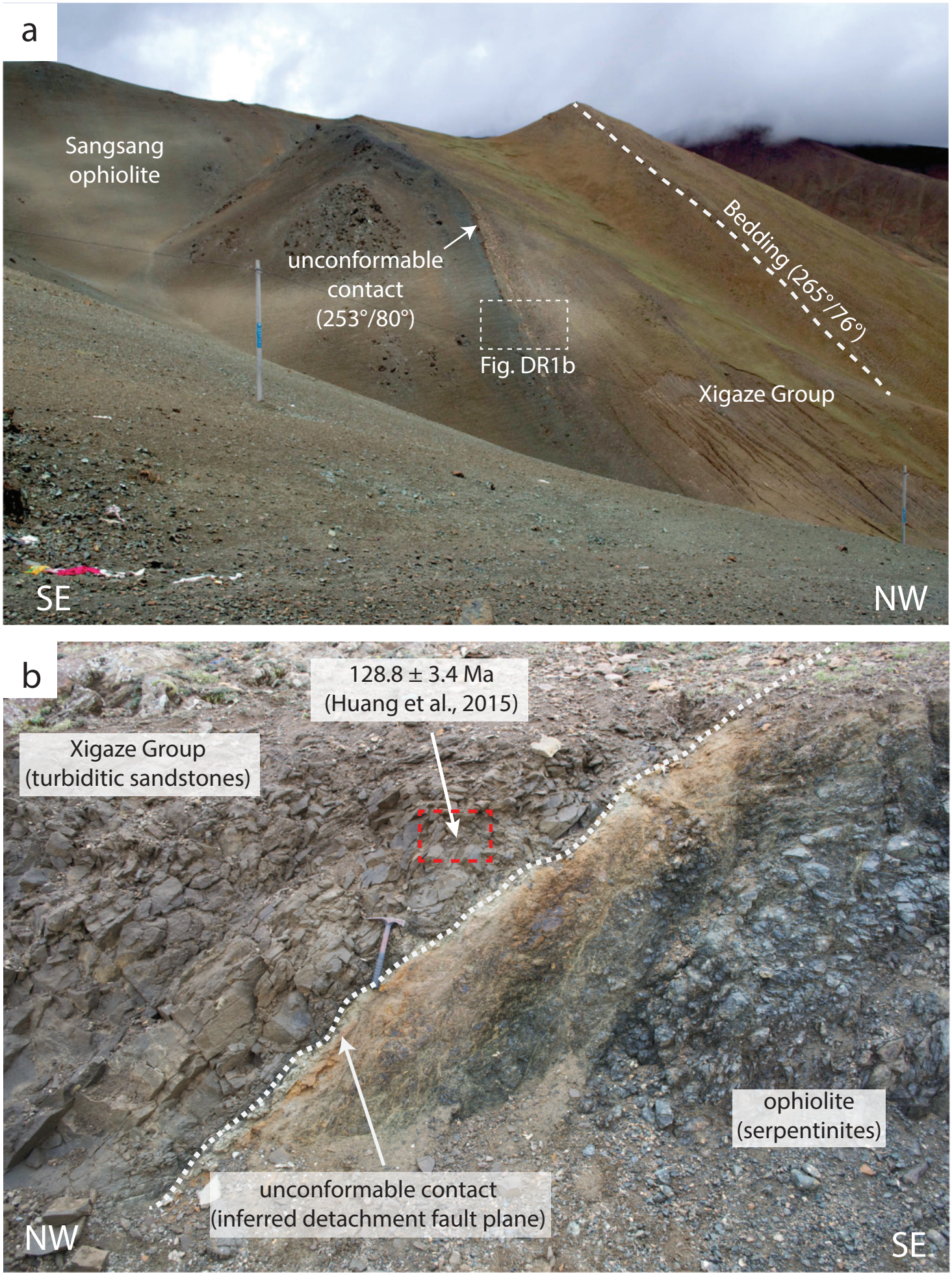
a
Sangsang
ophiolite
unconformable
contact
(253°/80°)
Fig. DR1b
Bedding (265°/76°)
Xigaze Group
SE
NW
b
128.8 ± 3.4 Ma
(Huang et al., 2015)
Xigaze Group
(turbiditic sandstones)
ophiolite
(serpentinites)
unconformable contact
(inferred detachment fault plane)
NW
SE

Figure DR2

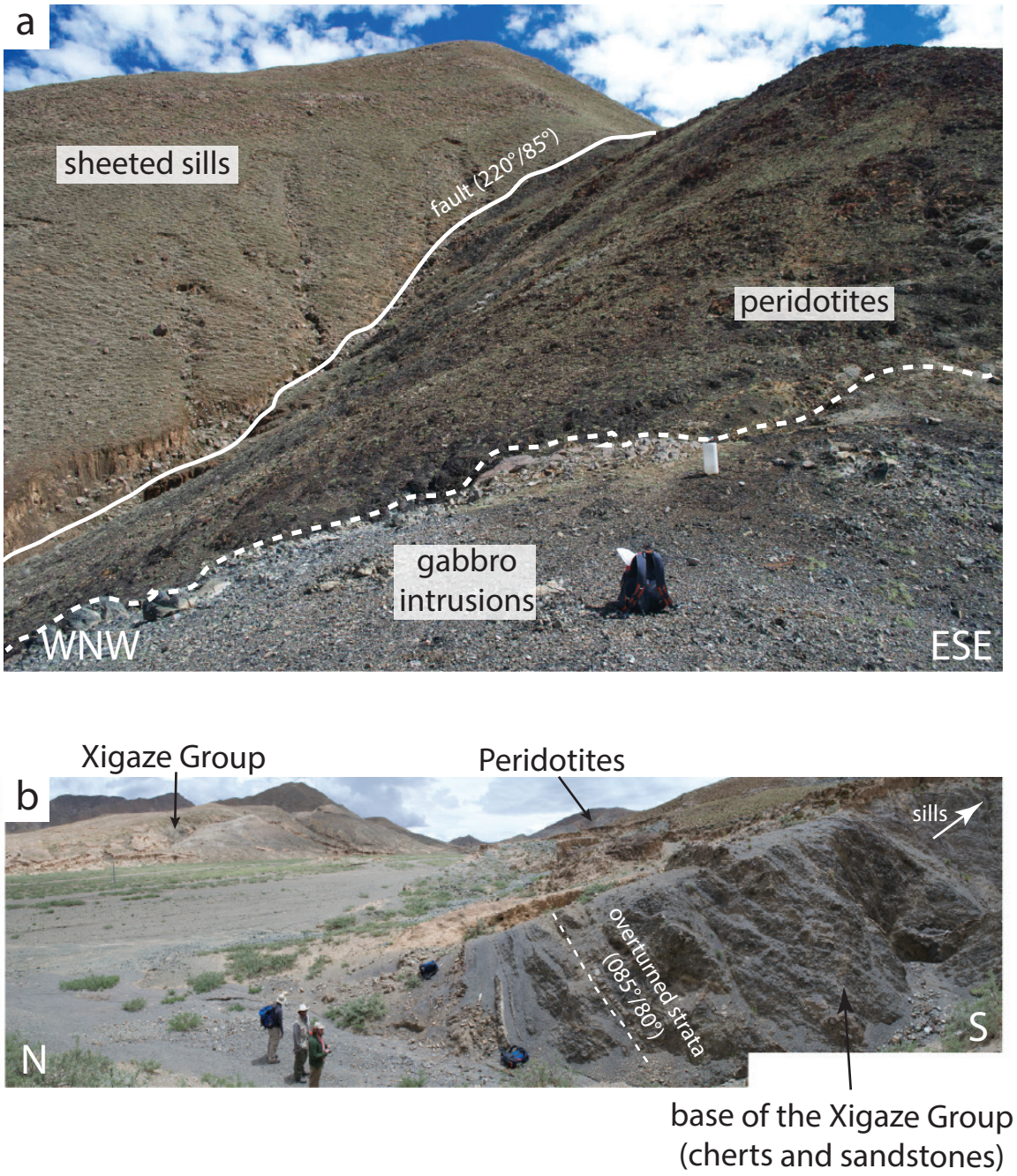
a
sheeted sills
fault (220°/85°)
peridotites
gabbro
intrusions
WNW
ESE
b
Xigaze Group
Peridotites
sills
overturned strata
(085°/80°)
N
S
base of the Xigaze Group
(cherts and sandstones)

Figure DR3

SANGSANG OPHIOLITE

Group 1
high coercivity/high blocking temperature

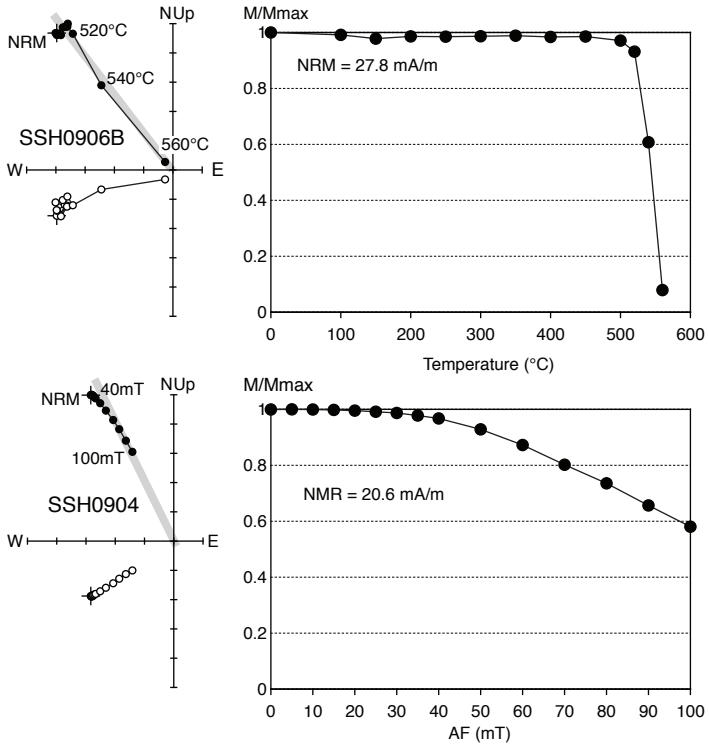

Group 2
low coercivity/high blocking temperature

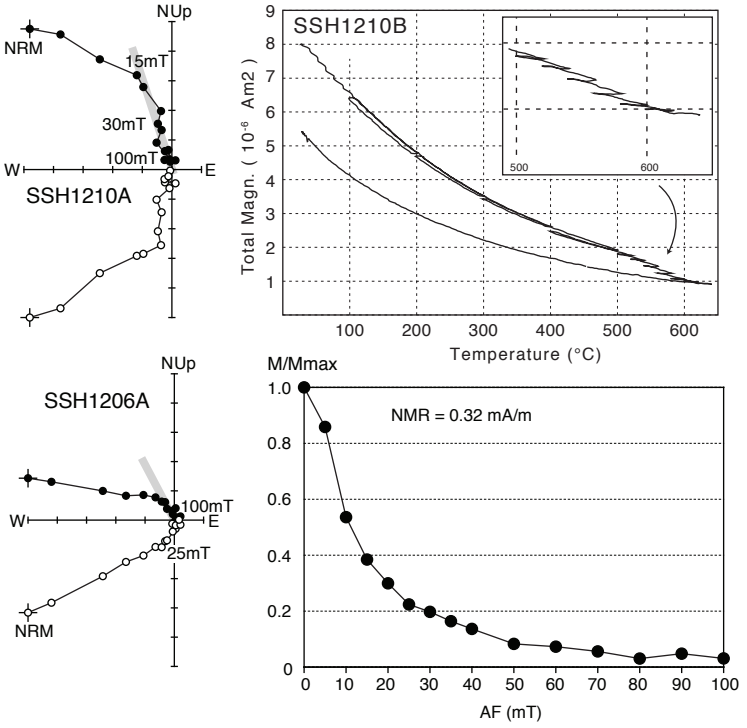

QUNRANG OPHIOLITE

GABBROS

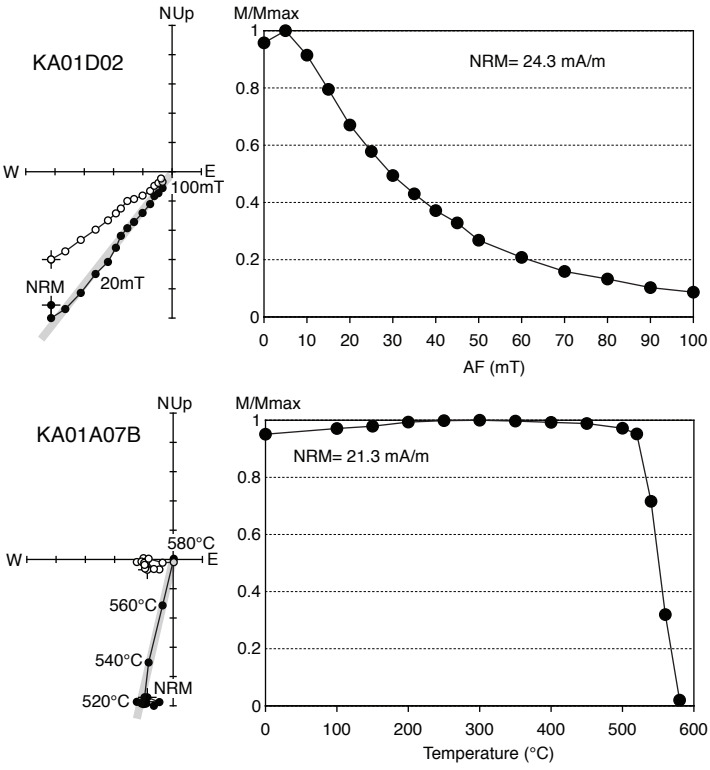

SHEETED SILLS

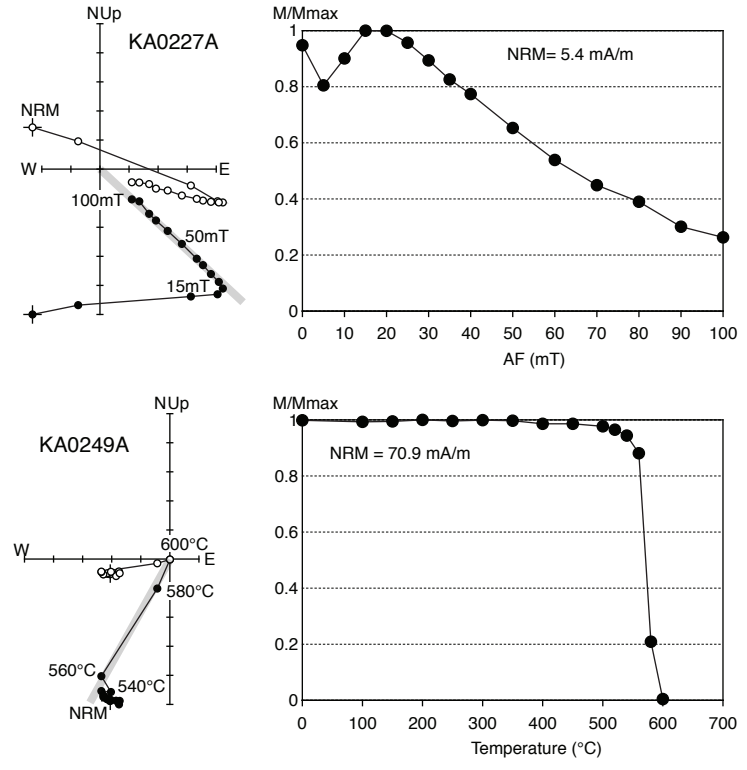

Figure DR4

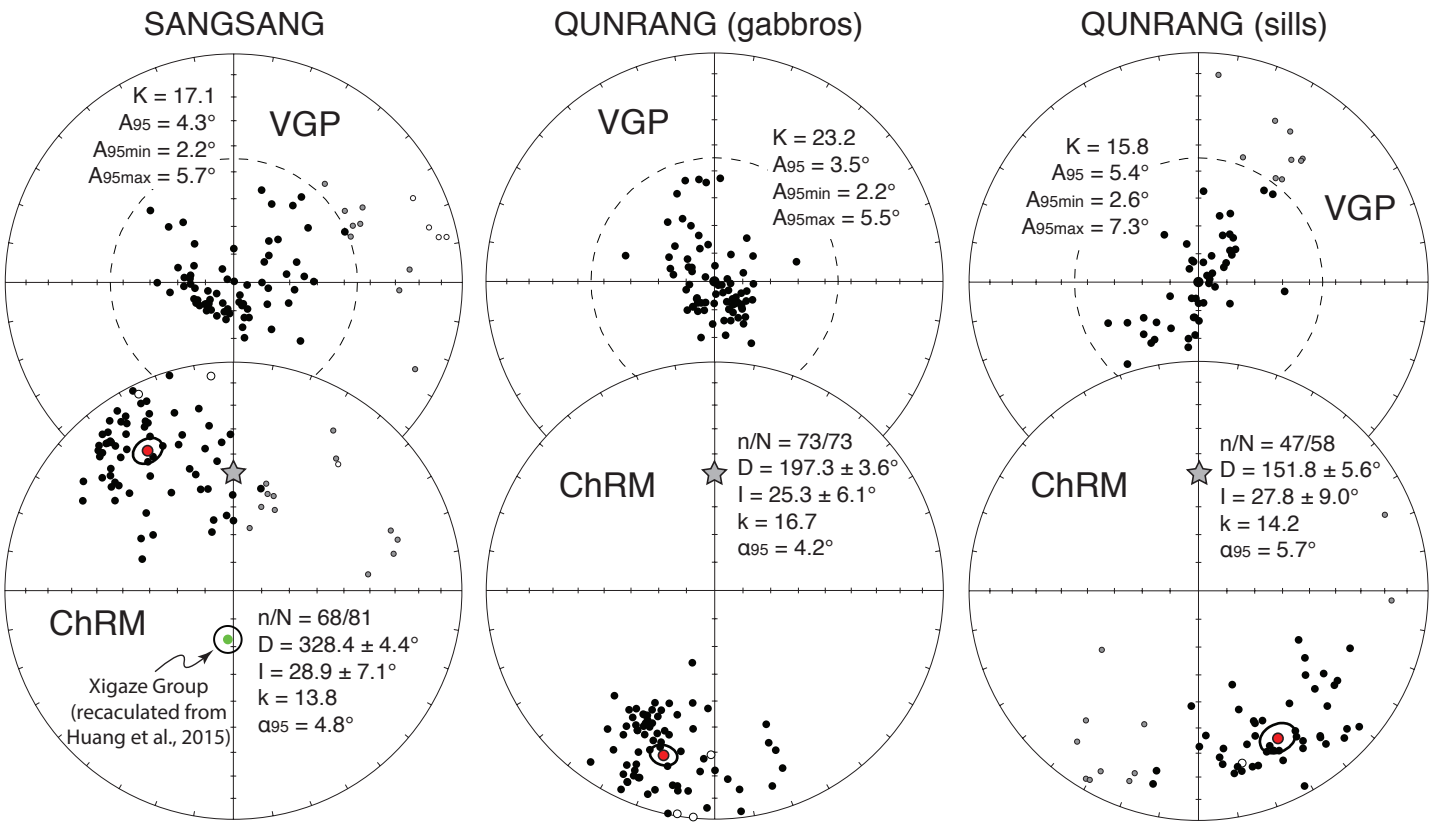
SANGSANG
K = 17.1
A95 = 4.3°
A95min = 2.2°
A95max = 5.7°
VGP
ChRM
n/N = 68/81
D = 328.4 ± 4.4°
I = 28.9 ± 7.1°
k = 13.8
α95 = 4.8°
Xigaze Group
(recaculated from
Huang et al., 2015)
QUNRANG (gabbros)
VGP
K = 23.2
A95 = 3.5°
A95min = 2.2°
A95max = 5.5°
ChRM
n/N = 73/73
D = 197.3 ± 3.6°
I = 25.3 ± 6.1°
k = 16.7
α95 = 4.2°
QUNRANG (sills)
K = 15.8
A95 = 5.4°
A95min = 2.6°
A95max = 7.3°
VGP
ChRM
n/N = 47/58
D = 151.8 ± 5.6°
I = 27.8 ± 9.0°
k = 14.2
α95 = 5.7°

Figure DR5

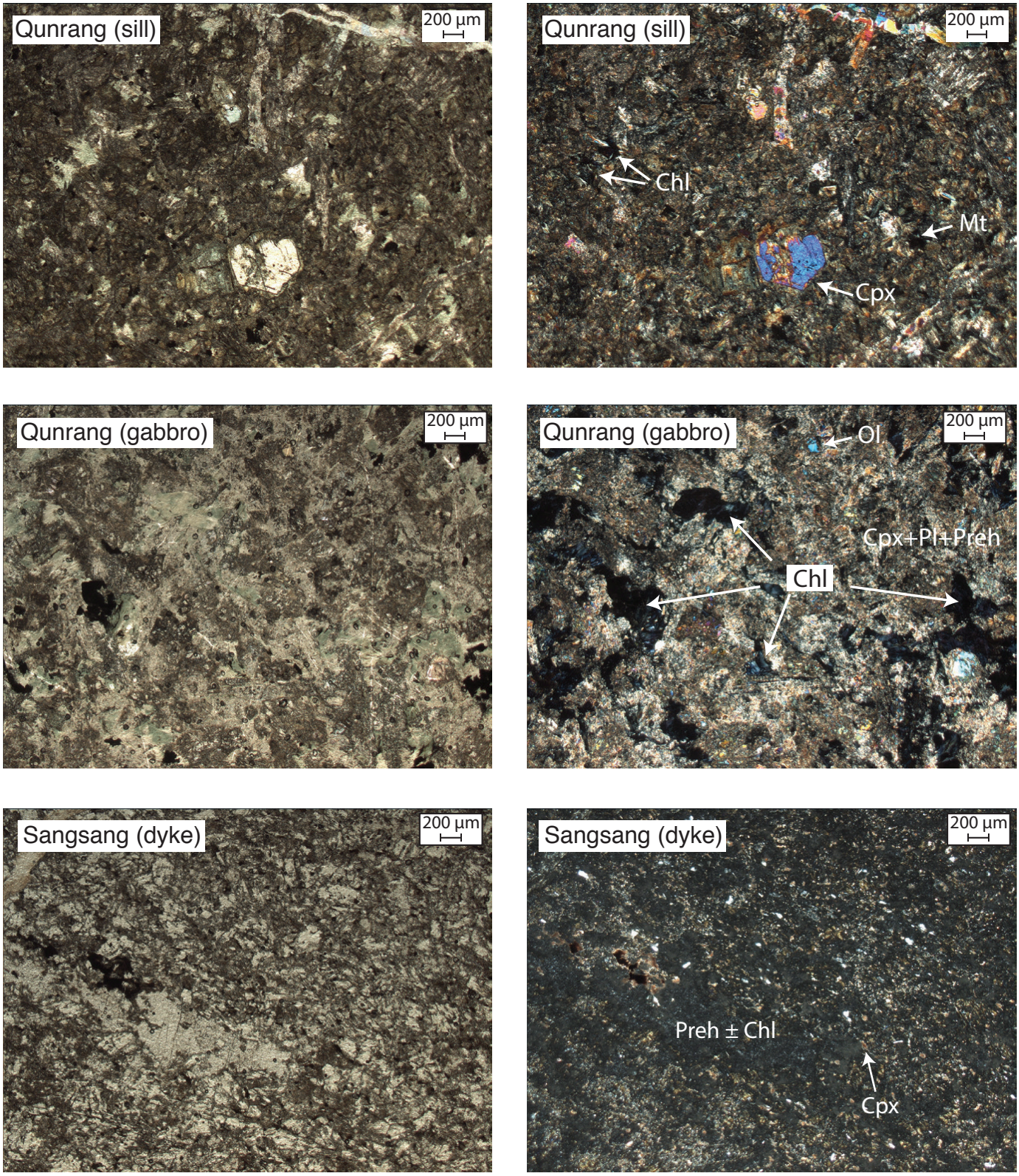
Qunrang (sill)
200 μm
Qunrang (sill)
200 μm
Chl
Mt
Cpx
Qunrang (gabbro)
200 μm
Qunrang (gabbro)
200 μm
Ol
Cpx+Pl+Preh
Chl
Sangsang (dyke)
200 μm
Sangsang (dyke)
200 μm
Preh ± Chl
Cpx

Figure DR6

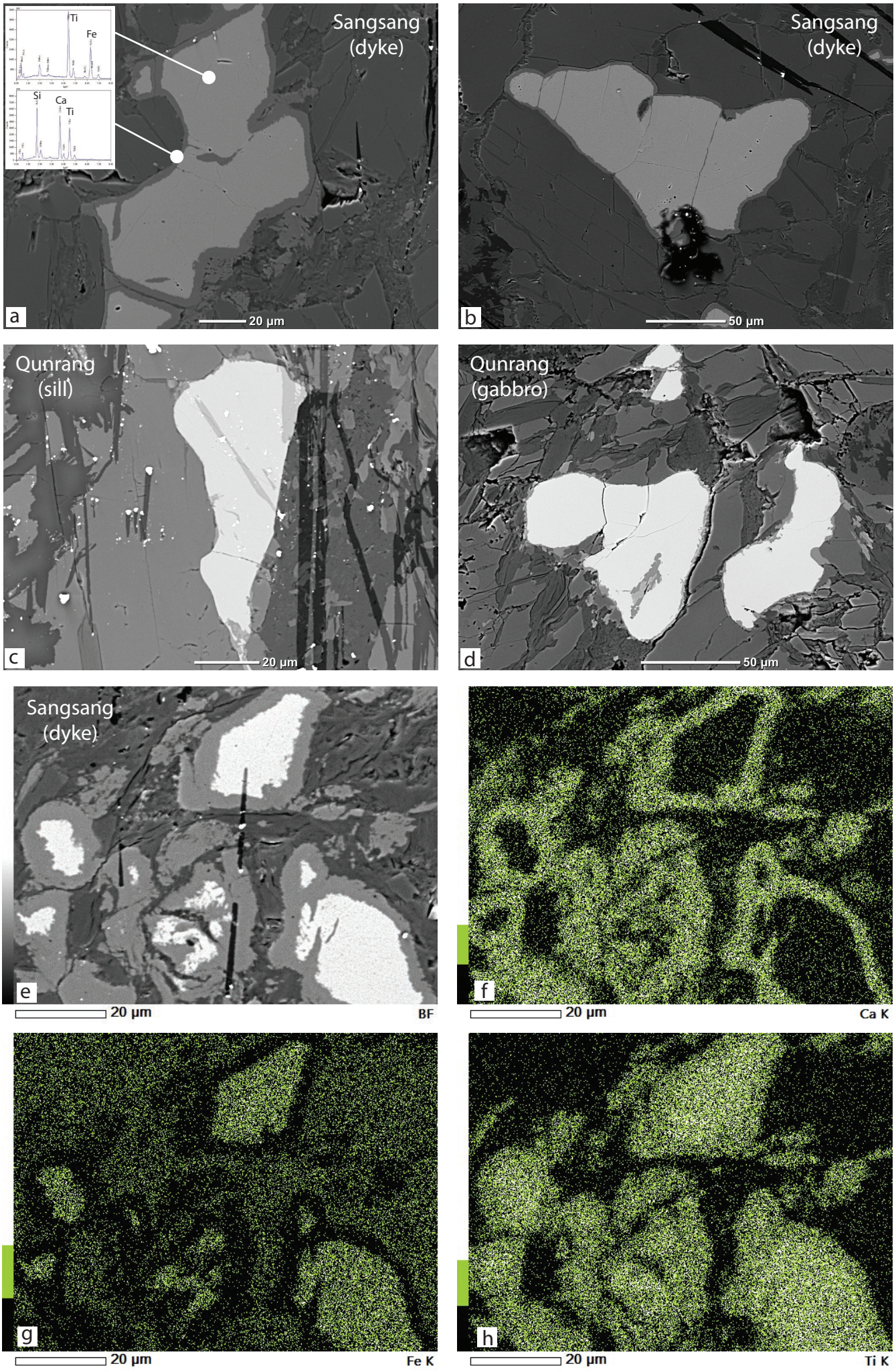
Sangsang
(dyke)
Ti
Fe
Si
Ca
Ti
a
20 μm
Sangsang
(dyke)
b
50 μm
Qunrang
(sill)
c
20 μm
Qunrang
(gabbro)
d
50 μm
Sangsang
(dyke)
e
20 μm
BF
f
20 μm
Ca K
g
20 μm
Fe K
h
20 μm
Ti K

Figure DR7

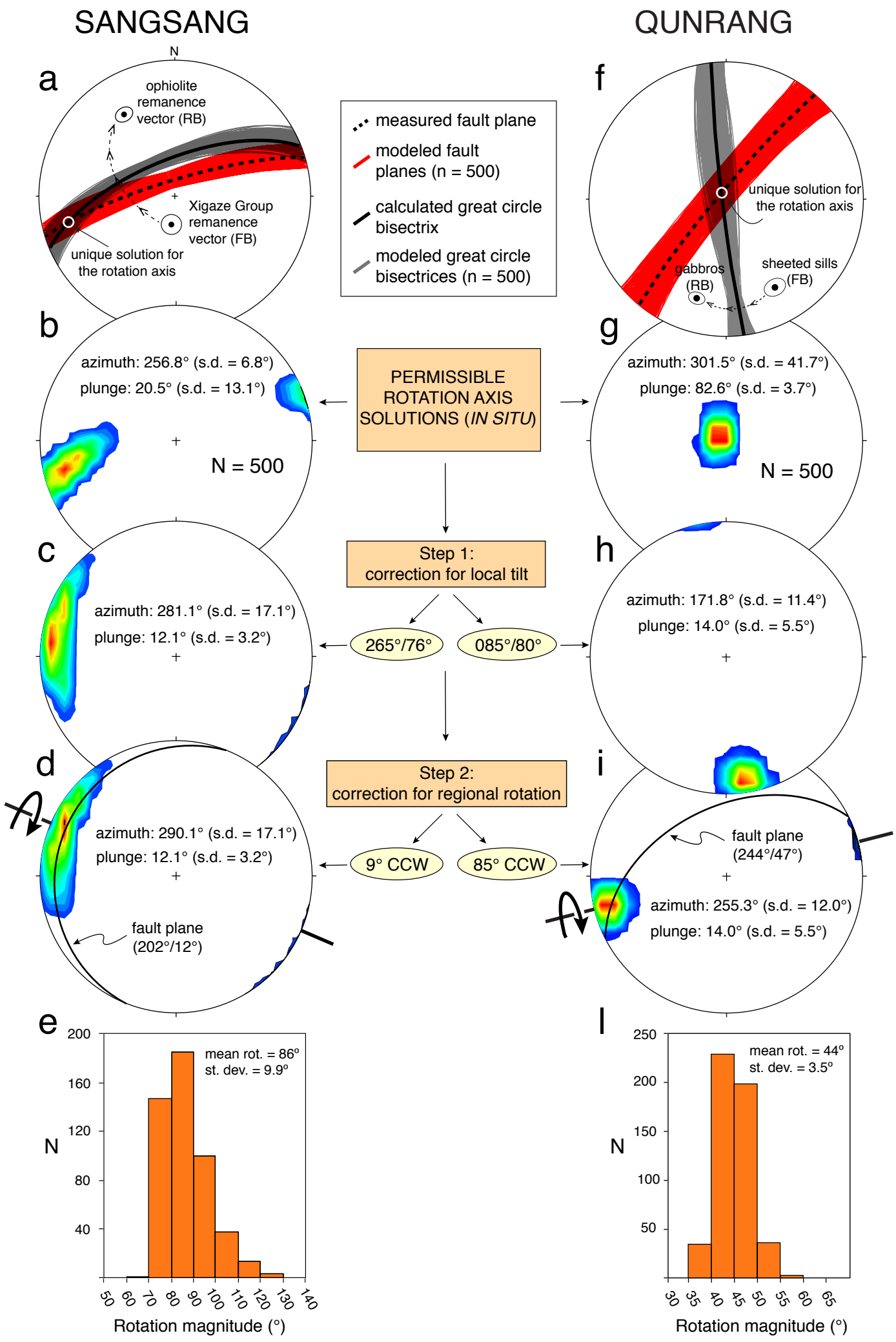
SANGSANG
QUNRANG
a
N
ophiolite remanence vector (RB)
Xigaze Group remanence vector (FB)
unique solution for the rotation axis
measured fault plane
modeled fault planes (n = 500)
calculated great circle bisectrix
modeled great circle bisectrices (n = 500)
f
unique solution for the rotation axis
gabbros (RB)
sheeted sills (FB)
b
azimuth: 256.8° (s.d. = 6.8°)
plunge: 20.5° (s.d. = 13.1°)
N = 500
PERMISSIBLE ROTATION AXIS SOLUTIONS (IN SITU)
g
azimuth: 301.5° (s.d. = 41.7°)
plunge: 82.6° (s.d. = 3.7°)
N = 500
Step 1: correction for local tilt
c
azimuth: 281.1° (s.d. = 17.1°)
plunge: 12.1° (s.d. = 3.2°)
265°/76°
085°/80°
h
azimuth: 171.8° (s.d. = 11.4°)
plunge: 14.0° (s.d. = 5.5°)
Step 2: correction for regional rotation
d
azimuth: 290.1° (s.d. = 17.1°)
plunge: 12.1° (s.d. = 3.2°)
9° CCW
85° CCW
fault plane (202°/12°)
i
fault plane (244°/47°)
azimuth: 255.3° (s.d. = 12.0°)
plunge: 14.0° (s.d. = 5.5°)
e
mean rot. = 86°
st. dev. = 9.9°
N
Rotation magnitude (°)
l
mean rot. = 44°
st. dev. = 3.5°
N
Rotation magnitude (°)

Table DR1. Paleomagnetic results from the Sangsang and Qunrang ophiolites.

Site	Lithology	Lat (°)	Long (°)	n/N	D (°)	I (°)	dDx (°)	dIx (°)	α_{95} (°)	k	K	A_{95} (°)	A_{95min} (°)	A_{95max} (°)
Sangsang														
SSH 06	Dyke	29.31887	86.61995	8/9	313.1	27.6	6.3	10.3	6.9	65.7	82.9	6.1	5.2	22.1
SSH 08	Dyke	29.31797	86.61989	11/13	338.8	23.8	5.5	9.4	7.2	40.7	73.9	5.3	4.6	18.1
SSH 09	Dyke	29.31797	86.61989	25/26	322.8	15.6	2.9	5.4	3.6	65.9	103.9	2.9	4.6	12.0
SSH 10	Dyke	29.31797	86.62010	5/6	340.0	48.5	23.3	23.4	21.2	14.0	15.3	20.2	6.3	29.7
SSH 11	Dyke	29.31768	86.61980	9/9	015.4	54.6	12.3	10.1	8.5	37.6	27.2	10.0	7.1	24.1
SSH 12	Dyke	29.31729	86.61996	12/12	331.6	46.2	13.2	14.2	11.1	16.1	14.8	11.7	4.4	17.1
SSH 13	Dyke	29.31889	86.61997	4/5	359.1	47.8	52.1	51.4	39.4	6.4	5.4	43.7	6.9	34.2
Mean values	Dykes			68/81	328.4	28.9	4.4	7.1	4.8	13.8	17.1	4.3	2.2	5.7
Qunrang														
KA 01A	Gabbro	29.20843	89.05311	11/11	178.9	9.2	9.8	19.2	12.7	14.0	22.7	9.8	4.6	18.1
KA 01B	Gabbro	29.20843	89.05311	17/17	206.2	38.7	4.2	5.5	4.1	76.1	86.1	3.9	3.9	13.8
KA 01D	Gabbro	29.20843	89.05311	21/21	197.2	13.1	5.5	10.6	5.7	32.0	34.4	5.5	3.6	12.0
KA 01F	Gabbro	29.20843	89.05311	24/24	200.7	32.5	5.1	7.6	4.9	38.1	38.3	4.8	3.4	11.1
Mean values	Gabbro			64/73	201.2	25.6	2.8	4.7	3.5	26.2	42.6	2.7	3.1	6.4
KA 02	Sheeted sills	29.20843	89.05311	47/58	151.8	27.8	5.6	9.0	5.7	14.2	15.8	5.4	2.6	7.3

n, number of specimens used for the computation of the mean values after filtering by a 45° cutoff. N, total number of specimens processed. D, I, in situ (geographic) mean declination and inclination. dDx, dIx, error margin of declination and inclination. α_{95} = semi-angle of the 95% confidence cone around the mean direction. k, precision parameter of the characteristic direction distribution. A_{95}, semi-angle of the 95% confidence cone around the mean virtual geomagnetic pole. K, precision parameter of the virtual geomagnetic pole distribution. A_{95min}, A_{95max}, minimum and maximum A_{95} value expected for a paleosecular variation-induced scatter, according to Deenen et al. (2011).